1-1-2019

CT Automated Exposure Control Using A Generalized Detectability Index

P. Khobragade
Marquette University

Franco Rupcich
GE Healthcare

Jiahua Fan
GE Healthcare

Dominic J. Crotty
GE Healthcare

Naveen M. Kulkarni
Medical College of Wisconsin

See next page for additional authors

Medical Physics, Vol. 46, No. 1 (January 2019): 140-151. DOI.

CT Automated Exposure Control Using A Generalized Detectability Index

P. Khobragade
Department of Biomedical Engineering, Marquette University and Medical College of Wisconsin, Milwaukee, WI
Franco Rupcich,
GE Healthcare, Waukesha, WI
Jiahua Fan
GE Healthcare, Waukesha, WI
Dominic J. Crotty
GE Healthcare, Waukesha, WI
Naveen M. Kulkarni
Medical College of Wisconsin, Milwaukee, WI
Stacy D. O'Connor
Medical College of Wisconsin, Milwaukee, WI
W. Dennis Foley
Medical College of Wisconsin, Milwaukee, WI
Taly Gilat Schmidt

Department of Biomedical Engineering, Marquette University and Medical College of Wisconsin, Milwaukee, WI

Abstract

Purpose

Identifying an appropriate tube current setting can be challenging when using iterative reconstruction due to the varying relationship between spatial resolution, contrast, noise, and dose across different algorithms. This study developed and investigated the application of a generalized detectability index (d'_{gen}) to determine the noise parameter to input to existing automated exposure control (AEC) systems to provide consistent image quality (IQ) across different reconstruction approaches.

Methods

This study proposes a task-based automated exposure control (AEC) method using a generalized detectability index (d'_{gen}). The proposed method leverages existing AEC methods that are based on a prescribed noise level. The generalized d'_{gen} metric is calculated using lookup tables of task-based modulation transfer function (MTF) and noise power spectrum (NPS). To generate the lookup tables, the American College of Radiology CT accreditation phantom was scanned on a multidetector CT scanner (Revolution CT, GE Healthcare) at 120 kV and tube current varied manually from 20 to 240 mAs. Images were reconstructed using a reference reconstruction algorithm and four levels of an in-house iterative reconstruction algorithm with different regularization strengths (IR1–IR4). The task-based MTF and NPS were estimated from the measured images to create lookup tables of scaling factors that convert between d'_{gen} and noise standard deviation. The performance of the proposed d'_{gen}-AEC method in providing a desired IQ level over a range of iterative reconstruction algorithms was evaluated using the American College of Radiology (ACR) phantom with elliptical shell and using a human reader evaluation on anthropomorphic phantom images.

Results

The study of the ACR phantom with elliptical shell demonstrated reasonable agreement between the d'_{gen} predicted by the lookup table and d' measured in the images, with a mean absolute error of 15% across all dose levels and maximum error of 45% at the lowest dose level with the elliptical shell. For the anthropomorphic phantom study, the mean reader scores for images resulting from the d'_{gen}-AEC method were 3.3 (reference image), 3.5 (IR1), 3.6 (IR2), 3.5 (IR3), and 2.2 (IR4). When using the d'_{gen}-AEC method, the observers' IQ scores for the reference reconstruction were statistical equivalent to the scores for IR1, IR2, and IR3 iterative reconstructions ($P > 0.35$). The d'_{gen}-AEC method achieved this equivalent IQ at lower dose for the IR scans compared to the reference scans.

Conclusions

A novel AEC method, based on a generalized detectability index, was investigated. The proposed method can be used with some existing AEC systems to derive the tube current profile for iterative reconstruction algorithms. The results provide preliminary evidence that the proposed d'_{gen}-AEC can produce similar IQ across different iterative reconstruction approaches at different dose levels.

1 Introduction

Radiation exposure from CT imaging is a growing public health concern, despite the benefits of CT imaging.[1], [2] Numerous methods have been developed to reduce CT radiation exposure such as automated exposure control (AEC),[3] organ-based tube current modulation,[4] iterative reconstruction algorithms,[5]-[7] and various image-based denoising techniques.[8]-[11] Automated exposure control techniques improve the consistency of image quality (IQ) by regulating the tube current across varying patient size, shape, and attenuation of anatomy. The tube current is modulated in the angular and/or longitudinal directions to account for the varying patient size and anatomy. Previous studies demonstrated that AEC methods can reduce patient radiation dose by 40% to 50% by modulating the tube current while maintaining sufficient IQ for the diagnosis.[12], [13]

CT manufacturers use different approaches for prescribing the target metric for the AEC system. Some manufacturers use noise index or noise standard deviation as the prescribed IQ descriptor,[3], [14] while others use a reference image or reference tube-current–time product as input to the AEC algorithm.[3], [15] In noise-descriptor-based AEC systems, the operator inputs the desired noise level, and the system is then calibrated for different patient sizes to derive the tube current profile to meet the prescribed level of IQ.

Noise-based AEC systems were initially designed for filtered back projection reconstruction, which is a linear reconstruction algorithm and for which noise standard deviation is inversely proportional to the square root of the radiation dose. However, this relationship is not necessarily valid when images are reconstructed using iterative reconstruction algorithms.[16]-[18] In addition, noise standard deviation does not fully describe overall IQ, as images with the same noise standard deviation but reconstructed by different algorithms may vary in noise texture, which affects the perceived IQ.[19]-[21]

Iterative reconstruction techniques have demonstrated substantial noise reduction potential,[22]-[24] which provides an opportunity to reduce CT radiation dose, with dose reduction varying from 50 to 82% across different algorithms and studies.[25] Unlike filtered back projection reconstruction, iterative reconstruction algorithms involve nonlinear processing and have different relationships between noise standard deviation and dose. Traditional metrics of IQ, such as noise and contrast-to-noise ratio, are insufficient for iterative reconstruction algorithms due to variations in noise texture and changes in spatial resolution with contrast.[25]-[27] Identifying an appropriate tube current setting may be challenging when using iterative reconstruction due to the varying relationship between noise, dose, and contrast across different iterative algorithms. For example, previous studies using human and model observers demonstrated decreased low-contrast detectability when using iterative reconstruction at low doses.[28] A previous study demonstrated using the Channelized Hotelling Observer (CHO) to optimize protocols and dose settings to maintain low-contrast detectability for iterative reconstruction.[29]

The purpose of this study was to investigate the application of a generalized detectability index (d'_{gen}) to automatically determine the noise parameter to input to existing AEC systems for different reconstruction approaches to obtain consistent IQ. The generalized detectability index is an IQ metric that considers spatial resolution, noise magnitude, noise texture, and the properties of the object to be detected. In the proposed approach, a desired d'_{gen} value is identified based on a reference noise level. The noise level needed to achieve this IQ level by a different reconstruction algorithm is then identified. In this work, the proposed d'_{gen}-AEC method was implemented by leveraging the noise-standard-deviation-based AEC that is available on some scanners, by using a lookup table of conversion factors that can be calculated by scanning the American College of Radiology (ACR) phantom.

The ability of the proposed d'_{gen}-AEC method to provide a desired IQ level over a range of iterative reconstruction algorithms was evaluated through a reader evaluation on phantom images and compared to a noise-standard-deviation-based AEC method.

2 Generalized detectability index (d'_{gen}) and proposed d'_{gen}-AEC method

The detectability index (d') is a task-based signal-to-noise ratio IQ metric that combines the contrast-dependent spatial resolution, noise properties, and an analytical representation of the task to be detected into a single figure of merit.**30**, **31** The detectability index d', corresponding to a non-prewhitening observer model, is expressed as

$$d'^2 = \frac{\left(\int\int W_{task}^2(u,v)MTF_{task}^2(u,v)dudv\right)^2}{\int\int W_{task}^2(u,v)MTF_{task}^2(u,v)\,NPS(u,v)dudv}$$

$$d'^2 = \frac{\left(\iint W_{task}^2(u,v)MTF_{task}^2\,(u,v)\,dudv\right)^2}{\iint W_{task}^2\,(u,v)MTF_{task}^2\,(u,v)\,NPS\,(u,v)\,dudv} \quad (1)$$

where W_{task} represents the frequency content of the signal, MTF_{task} is the modulation transfer function that represents how frequency content is transferred through the imaging system for a specific contrast level, and *NPS* is the noise power spectrum, which represents the noise variance across spatial frequencies. The d' metric has been used for various IQ studies, including evaluating the IQ and dose reduction potential of iterative reconstruction algorithms32-34 and for optimizing tube current modulation, reconstruction parameters, and gantry tilts in cone-beam CT.35

If the *NPS* is normalized by its integral across frequency, the *NPS* can be written as a product of the normalized *NPS*, *nNPS*, and noise variance, a^2, thereby separating noise magnitude from noise texture. With this modification, the expression for d' in Eq. 1 can be rewritten as

$$d'^2 = \frac{\left(\int\int W_{task}^2(u,v)MTF_{task}^2(u,v)dudv\right)^2}{\sigma^2\int\int W_{task}^2(u,v)MTF_{task}^2(u,v)\,nNPS(u,v)dudv}$$

$$d'^2 = \frac{\left(\iint W_{task}^2(u,v)MTF_{task}^2\,(u,v)\,dudv\right)^2}{\sigma^2\iint W_{task}^2\,(u,v)MTF_{task}^2\,(u,v)\,nNPS\,(u,v)\,dudv} \quad (2)$$

W_{task} is independent of radiation dose, but changes with the shape, size, and contrast of the object of interest. MTF_{task} and $nNPS$ are generally independent of dose for filtered back projection reconstruction, except at very low dose, for which electronic noise correction may be employed. For iterative reconstruction algorithms, the amount of blurring may vary with the dose/noise level. Previous work reported the behavior of nNP and MTF_{task} across a range of dose levels for the reference reconstruction algorithm and the four strengths of iterative reconstruction used in this study.36

Equation 2 can be written as:

$$d'^2_{gen} = \frac{K^2}{\sigma^2}$$

$$d'^2_{gen} = \frac{K^2}{\sigma^2} (3)$$

$$K^2 = \frac{\left(\int\int W^2_{task}(u,v) MTF^2_{task}(u,v) dudv\right)^2}{\int\int W^2_{task}(u,v) MTF^2_{task}(u,v)\, nNPS(u,v) dudv}$$

$$K^2 = \frac{\left(\iint W^2_{task}(u,v) MTF^2_{task}(u,v)\, dudv\right)^2}{\sigma^2 \iint W^2_{task}(u,v) MTF^2_{task}(u,v)\, nNPS(u,v)\, dudv} (4)$$

where K is a scalar conversion factor that depends on the reconstruction method and task object that is identified to represent IQ for a protocol, and d'_{gen} is the generalized metric, calculated using the scalar conversion factor, that we propose to represent overall IQ. Using Eq. 3, we can convert between noise standard deviation and the generalized detectability index for a specific reconstruction algorithm. This formulation enables identifying the noise standard deviation needed to produce a specific d'_{gen} value for a specific reconstruction algorithm using a precomputed lookup table of K scaling factors. Existing noise-based AEC methods can then be used to derive the tube current to provide this level of noise standard deviation. Iterative reconstruction algorithms may alter the perceived IQ by changing the noise texture and/or spatial resolution of the image. The proposed method is designed to adjust the standard deviation of the IR image to compensate for the changes in noise texture and spatial resolution to maintain the reference level of IQ.

Figure 1 presents a flowchart of the proposed d'_{gen}-AEC method for the case in which a reference noise level, or a reference image with acceptable IQ, is available for a reference reconstruction algorithm, for example, filtered back projection. The objective of the d'_{gen}-AEC system is to identify the noise standard deviation level required by an IR algorithm to provide d'_{gen} equivalent to the reference image or protocol. The method first requires that an object be identified to represent the IQ needs of the particular imaging task (task object). For tasks that require detection of low-contrast objects, such as a liver lesion evaluation, a low-contrast object of 20–40 mm size could be selected to represent the image feature whose visualization should drive the derivation of the tube current profile. For high-contrast detectability tasks, such as detecting contrast-filled vessels in CT angiography, a higher contrast object of 1–2 mm size could be selected to represent the image feature that should drive the derivation of the tube current profile. For combined tasks, the task with the higher current requirement should drive tube current selection. The proposed d'_{gen}-AEC method requires a lookup table of K-factors for the reference reconstruction algorithm and the desired IR algorithm. The generation of these K-factor lookup

tables will be described in Section 3. As illustrated in Fig. 1, the proposed d'_{gen}-AEC method consists of the following steps.

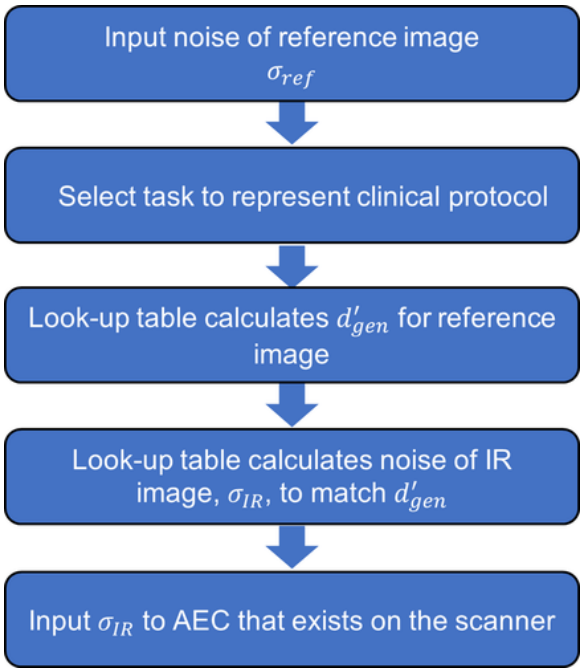

Figure 1 Flowchart of the proposed d'_{gen}-AEC method. [Color figure can be viewed at wileyonlinelibrary.com]

1. Identify the noise standard deviation of the reference image,$\sigma_{reference}$
2. Define an object to represent the imaging task, for example, size, contrast, and shape to be detected.
3. Calculate the **Figure 1** Flowchart of the proposed d'_{gen}-AEC method. [Color figure can be viewed at wileyonlinelibrary.com]
4. of the reference image using the Klookup table for the reference reconstruction algorithm and task object.

$$d'_{gen\_reference} = \frac{K_{reference\_taskobject}}{\sigma_{reference}}$$

$$d'_{gen\_reference} = \frac{K_{reference\_taskobject}}{\sigma_{reference}} \quad (5)$$

4. Calculate the standard deviation, σ_{IR}, required of the IR algorithm to meet this d'_{gen} level, using the Klookup table for the IR algorithm.

$$\sigma_{IR} = \frac{K_{IR\_taskobject}}{d'_{gen\_reference}}$$

$$\sigma_{IR} = \frac{K_{taskobject}}{d'_{gen\_reference}} (6)$$

The expressions in Eqs. 5 and 6 can be combined to relate the standard deviation of the iterative reconstruction to the standard deviation of the reference image at the same d'_{gen} level

$$\sigma_{IR} = \frac{K_{IR\_taskobject}}{K_{reference\_taskobject}} \sigma_{reference}$$

$$\sigma_{IR} = \frac{K_{IR\_taskobject}}{K_{reference\_taskobject}} \sigma_{reference} \quad (7)$$

5. Input the desired standard deviation of the IR algorithm, σ_{IR}, into the existing noise-based AEC system, which will derive the required tube current profile.

As can be seen in Eq. 7, the proposed method calculates the noise standard deviation of the IR algorithm required to meet the desired d'_{gen} IQ level by scaling the reference standard deviation.

3 Generation of *K*-factor lookup tables

The proposed d'_{gen}-AEC method requires lookup tables of the K scaling factors defined in Eq. 4, which depend on W_{task}, MTF_{task}, and $nNPS$, for each investigated reconstruction algorithm. W_{task} is analytically modeled based on the shape, size, and contrast of the task object to be detected, while MTF_{task} depends on the contrast of the task object.

In this study, MTF_{task} and $nNPS$ were estimated for each investigated reconstruction algorithm using the images of the ACR CT phantom. The ACR phantom was scanned on a clinical scanner (Revolution CT, GE Healthcare, Waukesha, WI) using the scan parameters and fixed tube current levels listed in Table 1. For each fixed tube current setting (20 to 160 mAs in steps of 20 mAs), 80 images were reconstructed at 2.5 mm slice thickness using the filtered back projection (FBP) reconstruction available on the scanner (Revolution CT, GE Healthcare), referred to as the reference protocol. Images at each tube current setting were reconstructed with four strengths of an in-house iterative reconstruction method (IR1–IR4), where a higher strength refers to more regularization. The IR algorithm used in this study contains advanced noise modeling and object modeling. To speed up the reconstruction process, the system optics modeling is simplified in the algorithm, as this is the most time-consuming portion of a model-based iterative reconstruction method. This IR algorithm has achieved similar reconstruction speed as FBP.

Table 1. Summary of CT acquisition parameters and experimental conditions. All scans were performed on a clinical CT scanner (Revolution CT, GE Healthcare). For Studies 2 and 3, the tube current profile was derived by the automated exposure control (AEC) on the scanner (SmartmA) from the prescribed noise indices (see Sections 5 and 6)

	***K*-factor lookup table generation**	**Study 1: evaluation for case of ideal noise-based AEC**	**Study 2: evaluation using existing noise-based AEC**	**Study 3: evaluation using human reader evaluation**
Tube voltage (kV)	120	120	120	120
Tube current time product (mAs)	20–160 in steps of 20	20–240 in steps of 20	Prescribed noise index varied for each case (18 HU reference)	Prescribed noise index varied for each case (17 HU reference)
AEC method	Fixed tube current	Fixed tube current	SmartmA	SmartmA
FOV (cm)	25 × 25	25 × 25	25 × 25	35 × 35
Pixel size (mm)	0.49 × 0.49	0.49 × 0.49	0.49 × 0.49	0.68 × 0.68
Slice thickness (mm)	2.5	2.5	2.5	2.5
Phantom	ACR	ACR ACR + 25 × 35 cm shell	ACR + 25 × 35 cm shell	Abdominal phantom with liver lesions

Task object shape, diameter (mm), contrast (HU)	Gaussian, 25, 120 Disk, 25, 120 Gaussian, 5, 955 Disk, 5, 955	Gaussian, 25, 120	Gaussian, 25, 120	Gaussian, 25, 120

The task-based MTF, MTF_{task}, represents the spatial resolution of the system for a specific contrast level. MTF_{task} is used in this study instead of the traditional definition of MTF to more accurately represent the nonlinear response of iterative reconstruction algorithms. To incorporate the effect of contrast-dependent resolution, MTF_{task} was obtained by estimating the edge spread function from the bone and acrylic contrast elements in Module 1 of the ACR phantom using previously published methods.**26** Estimation of the edge spread function incorporates resolution information from both spatial directions within the image slice. NPS was calculated from the uniform section of Module 3 of ACR phantom. A total of 200 ROIs of 128 × 128 pixels from 50 axial image slices were used to calculate the NPS. The mean value of each selected ROI was subtracted prior to the Fourier transform step to set the zero frequency value to zero.

W_{task} is the analytical function that describes the spatial frequency content of the signal, including its size, shape, and contrast. The task object should have the same contrast level as the contrast element used to estimate MTF_{task}, but can be of different size or shape to better reflect the needs of the specific protocol. A Gaussian-shaped signal may be a reasonable model for contrast-enhanced lesions in which the enhancement increases toward the center of the lesion, for example, in tumors where the vasculature may be denser near the center and decreasingly so toward the periphery. For other signals, such as a contrast-filled vessel, a disk-shaped object may be more appropriate. Equation 8 expresses the 2D Gaussian in image space that was used to represent $W_{task}\ (x, y)$ in a previous study of CT IQ,**34**

$$W_{task}(x, y) = C \exp\left(-\frac{x^2 + y^2}{FWHM^2}\ln(2)\right).$$

$$W_{task}(x,y) = C\ \exp\left(-\frac{x^2+y^2}{FWHM^2}\ln(2)\right) \quad (8)$$

In this study, *K*-factor lookup tables were generated for both a 120 HU, 25-mm-diameter signal (e.g., abdomen/liver protocol) and a 955 HU, 5-mm-diameter signal (e.g., angiography protocol). *K*-factor lookup tables were calculated assuming both a Gaussian-shaped signal [Eq. 8 with FWHM = diameter] and a constant disk-shaped signal with the corresponding diameter.

Figure 2 plots the *K*-factors [Eq. 4] obtained for the reference reconstruction algorithm and four levels of IR for a 25-mm-diameter task with 120 HU contrast and 5-mm-diameter task with 955 HU contrast, modeled using both Gaussian and disk shapes. The plots demonstrate a decrease in *K*-factors at lower dose levels for some reconstruction methods that were due to changes in the $nNPS$ and MTF_{task} at lower dose levels. However, the *K*-factors were relatively constant across a wide range of dose values. Therefore, for each reconstruction algorithm, the average *K*-factor across the measured dose values was used as the final lookup table for subsequent evaluation.

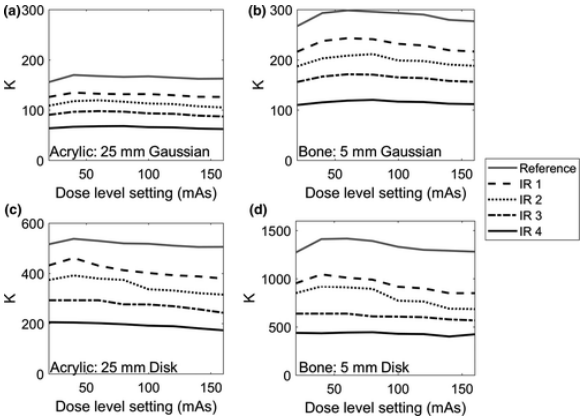

Figure 2 *K*-factors for the (a) 25-mm diameter acrylic task and (b) 5-mm diameter bone task, modeled with a Gaussian shape, plotted across the range of dose levels for each reconstruction method. *K*-factors for the (c) 25-mm diameter acrylic task and (d) 5-mm diameter bone task, modeled with a disk shape, plotted across the range of dose levels for each reconstruction method. Note the higher amplitude of *K*-factors for the disk-shaped objects compared to the Gaussian objects.

The *K*-factors calculated assuming the disk shape have higher amplitude than the *K*-factors calculated assuming the Gaussian shape, due to the higher frequency content of the sharp transition in the disk shape. As seen in Eq. 7, the ratio of the *K*-factors for the IR algorithm relative to the reference algorithm determines the final weighting of the reference noise standard deviation. To understand the effect of task shape on the ratio of *K*-factors for the IR algorithms relative to the reference algorithm, Fig. 3 plots the ratio of K_{IR} to $K_{reference}$ for the IR algorithms and the two task shapes. The task shape had a small effect on the *K*-factor ratios for the 25-mm-diameter acrylic task object, with a larger effect for the 5-mm bone task object, due to the increased high frequency content for this smaller object with higher contrast.

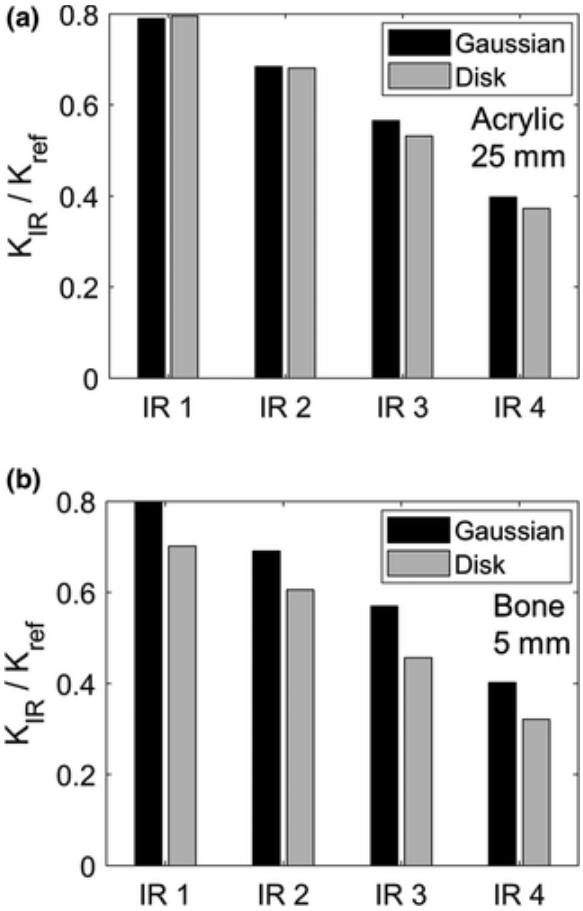

Figure 3 (a) Ratio of *K*-factors (iterative/reference) for the 25-mm diameter acrylic task modeled by both Gaussian and disk shapes. (b) Ratio of *K*-factors (iterative/reference) for the 5-mm diameter bone task modeled by both Gaussian and disk shapes.

Determining the correct tube current setting for low-contrast tasks is particularly challenging for IR algorithms because the MTF response of the algorithm can decrease at low-contrast levels.**34** Therefore, the following studies investigated the performance of the d'_{gen}-AEC method while representing the task object as the 25-mm-diameter acrylic object. As both Gaussian and disk shapes resulted in similar *K*-factor ratios for this larger task object, the Gaussian lookup table was used for the subsequent studies.

4 Study 1: evaluation of d'_{gen}-AEC method for case of ideal noise-based AEC

4.A. Study 1: methods

The first set of experiments were designed to validate whether an image with noise standard deviation suggested by the *K*-factor lookup tables provided the desired d' IQ level. In this study, the ACR phantom, without and with elliptical shell of diameters 25 cm × 35 cm (Fig. 4), was scanned using parameters listed in Table 1. The tube current was fixed for each scan (i.e., no AEC), with the tube current setting varied from 20 to 240 mAs in increments of 20 mAs across scans. Using the ACR phantom in this study enables comparing the d'_{gen} values predicted by the lookup table with the d' values measured directly from the image data using the methods described in Section 3. Throughout the paper, d'_{gen} represents the detectability calculated using the lookup table *K*-factor and the noise standard deviation estimated in the image [Eq. 3]. d' represents the

detectability measured from image data [Eq. 2]. Repeating the experiment using the ACR phantom with elliptical shell enables evaluating the accuracy of the predicted d'_{gen} values for an object that is different than the one used to generate the lookup tables.

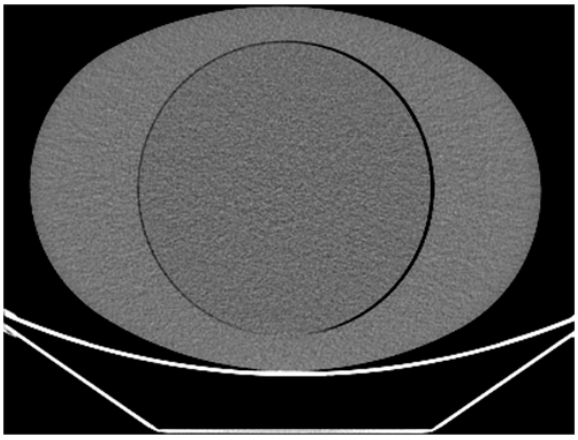

Figure 4 Image demonstrating the size and shape of the elliptical shell used with the ACR phantom for Studies 1 and 2.

At each dose level, images were reconstructed using the reference reconstruction algorithm and the four levels of IR. The noise standard deviation was calculated in a 128 × 128 ROI extracted from the uniform region of ACR phantom for each reconstruction algorithm and dose level. For each reconstruction algorithm, d'_{gen} was calculated using the measured noise standard deviation at each dose level and the dose-independent *K*-factor lookup tables for the acrylic task. The d' was also measured directly from the image data, using the methods described in Section 3, for each reconstruction algorithm and dose level, and for the ACR phantom with and without shell. The predicted d'_{gen} and measured d' values were compared across the dose range to evaluate the accuracy of the d'_{gen} values obtained using the *K*-factor lookup tables.

This dataset was also used to evaluate the proposed d'_{gen}-AEC method for the case of an ideal noise-based AEC method that can derive the tube current profile to exactly provide the desired noise standard deviation for each reconstruction approach. The reference protocol was selected as the 240 mAs acquisition of the ACR phantom with elliptical shell reconstructed with the FBP reference algorithm and 2.5-mm slice thickness. The representative W_{task} was selected as a 25-mm Gaussian with 120 HU contrast. The reference noise standard deviation, $\sigma_{reference}$, was measured in the images to be 23.6 HU. Using this standard deviation and the *K*-factor lookup table for the reference algorithm, the reference d'_{gen} was calculated to be 4.8. For each IR algorithm, the standard deviation required to match the d'_{gen} of the reference image, σ_{IR}, was calculated using the *K*-factor lookup tables calculated in Section 7. For each IR algorithm, the dataset with standard deviation of σ_{IR} was identified from the acquired set of images and the d' was calculated from the image data using the methods described in Section 3. The d' values estimated from the image data were compared to the desired, reference d'_{gen} for each IR algorithm.

4.B. Study 1 results

Figure 5 plots the d'_{gen} predicted by the *K*-factor lookup table and d'measured in the image data for the ACR phantom with and without elliptical shell for the IR 2 reconstruction algorithm. Similar results were obtained for the other reconstruction approaches. Reasonable agreement between the predicted and measured detectability was observed, with a maximum error of 45%

for the elliptical phantom with shell at low dose and a mean absolute error of 15% across all dose levels. The difference between the predicted and measured detectability increased with decreasing dose for the elliptical phantom. With the elliptical shell, the exposure reaching the detector at the low-dose levels is less than the exposures that were used to create the lookup table without the shell. Figure 2 demonstrated a small decrease in the K-factors at lower dose for the ACR phantom without shell. It is possible that the K-factors decrease more substantially at the detected exposure levels corresponding to low-dose acquisitions of the elliptical phantom. Therefore, the assumption of constant K-factors may introduce greater error for low-dose acquisitions of larger objects. Despite this error at low-dose levels, the results of the ACR phantom with elliptical shell demonstrate that the lookup table method provides reasonably accurate measured d' values for an object that is different than the one used to create the lookup tables.

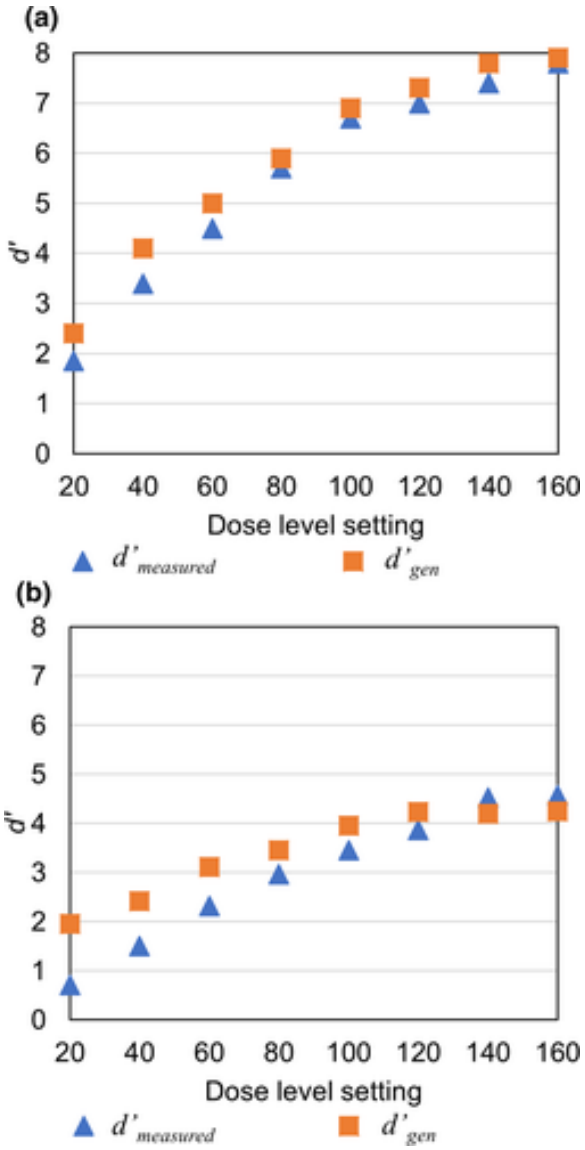

Figure 5 Prescribed d'_{gen} and measured d'_{gen} for images of the (a) ACR phantom and (b) ACR phantom with elliptical shell plotted across a range of dose levels for IR 2. [Color figure can be viewed at wileyonlinelibrary.com]

Figure 6 presents the images of the ACR phantom with elliptical shell resulting from the proposed d'_{gen}-AEC method for the case of an ideal noise-based AEC system that can provide images with the prescribed noise standard deviation. Figure 6 presents the reference image as

well as the images resulting from IR 2 and IR 4 for two cases: (a) tube current setting manually identified to match the d'_{gen} of the reference image (b) tube current setting manually identified to match the noise standard deviation of the reference image. The d'calculated from the image data was 4.8 for IR 2 and 4.7 for IR 4 for the d' matched images, compared to the prescribed reference d'_{gen} of 4.8, demonstrating that the proposed lookup tables can match the prescribed d'_{gen}value for the case of an ideal noise-based AEC. The images resulting from matching the noise standard deviation of the reference scan resulted in d' values of 2.9 (IR 2) and 1.2 (IR 4), suggesting reduced IQ for the iterative algorithms when matching noise standard deviation of the reference scan. Matching the d'_{gen} of the reference scan required more dose than matching the noise standard deviation, as seen in Fig. 6. However, both iterative reconstruction algorithms matched the d' of the reference image while reducing the dose compared to the reference reconstruction algorithm.

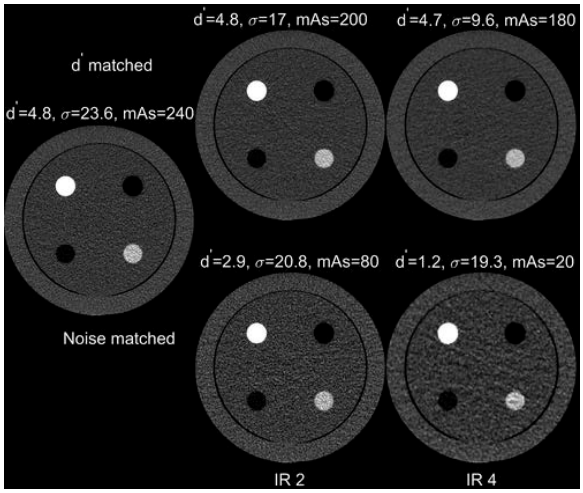

Figure 6 The reference image of the ACR phantom with elliptical shell is displayed at the left side of the figure. The top row shows images with noise standard deviation identified to match the d'_{gen} of the reference image for IR 2 and IR 4. The bottom row shows images with noise standard deviation identified to match the noise standard deviation of the reference image. The prescribed d'_{gen} was equal to 4.8. The d' calculated from the image data, as well as the noise standard deviation and tube current setting, is displayed above each image. Because of the 25 × 25-cm FOV, the full extent of the elliptical shell is not visible in the images.

5 Study 2: evaluation of d'_{gen}-AEC combined with existing noise-based AEC method

5.A. Study 2: methods

The next study evaluated whether the proposed d'_{gen}-AEC method, combined with the noise-based AEC available on the scanner, can produce IQ equivalent to the reference image across the investigated iterative reconstruction algorithms. The ACR phantom with elliptical shell was scanned using the existing tube current modulation AEC (SmartmA) at a reference protocol with prescribed noise standard deviation of 18 HU and reference FBP reconstruction (Table 1). Using $\sigma_{reference} = 18$ HU and the K-factor lookup tables (W_{task} corresponding to 25-mm Gaussian with 120 HU contrast), the reference d'_{gen} was calculated to be 7.15. For each level of iterative reconstruction, the K-factor lookup tables were used to calculate the noise standard deviation, σ_{IR}, required to obtain the reference d'_{gen} of 7.15. For each iterative reconstruction algorithm (IR1–IR4), the phantom was scanned with the σ_{IR} value as the noise standard deviation input to the

scanner AEC system. For comparison, the phantom was also scanned for each IR algorithm with the reference noise standard deviation, $\sigma_{reference} = 18$ HU, as the noise level input to the AEC system. For each case, the d' was calculated from the reconstructed images using the methods described in Section 3 and compared to the desired reference d'_{gen} value predicted by the *K*-factor lookup table.

5.B. Study 2: results

Figure 7 presents the results of the d'_{gen}-AEC method when combined with existing noise-based AEC system. Figure 7 presents the reference image as well as the images resulting from the four IR levels with the prescribed noise level selected to match the d'_{gen} (top row) of the reference image and the noise standard deviation (bottom row) of the reference image. Table 2 lists the prescribed d'_{gen}, measured d', prescribed noise standard deviation, and measured noise standard deviation for each image displayed in Fig. 7.

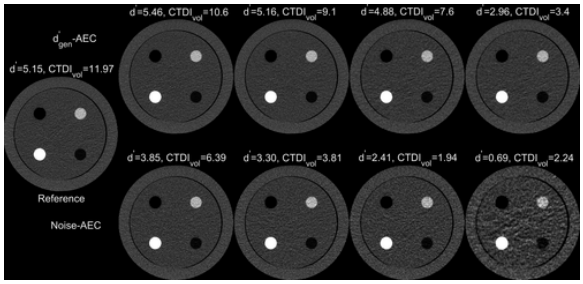

Figure 7 The reference image is displayed at the left side of the figure. The top row displays images resulting from the proposed to d'_{gen}-AEC method, where the prescribed noise level was calculated using the *K*-factor lookup to match the d'_{gen} of the reference image and the existing AEC system was used to derive the tube current profile to meet that noise level. The bottom row displays images generated by prescribing the same noise level as the reference image. The images, from left to right, represent IR 1, IR 2, IR 3, and IR 4. The d' calculated from the image data and $CTDI_{vol}$ are displayed above each image. The prescribed d'_{gen} was equal to 7.15. The prescribed and measured noise values for the d'_{gen}-AEC method are given in Table 2.

Table 2. The prescribed d'_{gen}, measured d', prescribed noise standard deviation, and measured noise standard deviation tabulated for each reconstruction approach in Fig. 7. The resulting d'_{gen}, calculated by the lookup table for the measured noise standard deviation, is also presented to evaluate the error due to the lookup table

	Prescribed d'_{gen}	Measured d'	Prescribed σ	Measured σ	d'_{gen} resulting from measured σ
Reference	7.1	5.15	18	21.16	5.7
IR 1	7.1	5.41	14.5	18.27	5.6
IR 2	7.1	5.15	12.4	15.81	5.6
IR 3	7.1	4.86	10	13.71	5.2
IR 4	7.1	2.93	7	12.77	3.9

As seen in Table 2, there were discrepancies between the prescribed $d'_{gen}$and measured d' values, with errors ranging from 24% to 31% for the reference IR1–IR3 algorithm and 58% error for IR 4. The ability of the d'_{gen}-AEC method to produce the desired d' depends on (a) the accuracy of the *K*-factor lookup table approximation which was quantified in Section 4 and (b) the accuracy of the measured noise compared to the requested noise level. The results in this section include both sources of error. To further analyze the sources of error, Table 2 lists the prescribed (σ_{IR}) and

measured (σ) noise standard deviation, with higher error between prescribed and measured noise associated with increasing levels of applied iterative reconstruction. To further explore the source of discrepancy between the prescribed d'_{gen} and measured d' values, Table 2 also lists the d'_{gen} values predicted by K-factor lookup table for the measured noise level, with errors ranging from 3% for IR 2 to 25% for IR 4. The results suggest that the agreement between the prescribed d'_{gen} and measured d' values across the wide range of applied iterative reconstruction levels depends on the accuracy of the measured vs prescribed noise values across those same levels. The AEC algorithm is not typically defined for the phantom used in this specific experiment but, despite these errors, Fig. 7 demonstrates that the d'_{gen}-AEC method provides more consistent IQ compared to the reference scan than the approach of matching the noise standard deviation of the reference scan at dose levels that are reduced compared to the reference scan. As seen in Fig. 7, matching the noise standard deviation of the reference scan required less dose than matching the $d'_{gen}$of the reference scan but resulted in lower d' values.

6 Study 3: evaluation of d'_{gen}-AEC using an anthropomorphic phantom and human reader evaluation

6.A. Study 3: methods

Experiments with an anthropomorphic phantom were performed to evaluate whether the d'_{gen}-AEC method produces images reconstructed by iterative algorithms that have equivalent subjective IQ to the reference scan, as evaluated by expert human readers. This study used an upper abdominal phantom representing a small adult (CT Torso Phantom, CTU-41, Kyoto Kagaku, Kyoto, Japan), with low-contrast structures in the liver and with approximate diameters of 14 cm (anteroposterior) and 20 cm (lateral), as measured on the image slice used for IQ evaluation. The phantom was first scanned on the clinical scanner using the existing AEC at a selected reference protocol of prescribed noise level of 17 HU and reference FBP reconstruction (Table 1). Using the steps shown in Fig. 1, the d'_{gen}-AEC method determined the noise index level to input into the existing AEC system (SmartmA) for the four levels of an in-house iterative reconstruction algorithm (IR 1, IR 2, IR 3, IR 4) to match the d'_{gen} of the reference image. This study used the K-factor lookup tables assuming the 25-mm Gaussian task object with 120 HU contrast. In this study, the low-contrast objects within the abdominal phantom (various liver lesions with ~25 HU contrast) were different than the task object used to determine the K-factor lookup table. Therefore, this study investigated whether the d'_{gen}-AEC can provide comparable IQ across reconstruction approaches without exact knowledge of the task object. For comparison, the anthropomorphic phantom was also scanned at a prescribed noise level of 17 HU using the existing AEC algorithm (SmartmA) for the four levels of iterative reconstruction.

Three board-certified radiologists with expertise in abdominal/body imaging and two clinical application specialists in CT imaging, each with more than 30 yr of experience, evaluated the images for overall diagnostic IQ, image noise level, and noise texture on 5-point Likert scales (Table 3). The observers were blinded to the radiation dose and reconstruction method.

Table 3. Likert score used to evaluate the overall image quality (IQ), noise magnitude, and noise texture

Likert scale	Overall IQ	Noise magnitude	Noise texture
1	Insufficient for diagnosis	Too much, cannot discern basic structure	Noise texture can easily mistake as pathology

2	Degraded IQ barely sufficient for diagnosis	Distracting, barely sufficient for diagnosis	Noise texture may be questioned as pathology
3	Satisfactory, fully adequate for diagnosis	Satisfactory, fully adequate for diagnosis	Noise texture not ideal but sufficient for diagnosis
4	Above average IQ	Would consider lowering dose	Normal noise texture
5	Excellent IQ	Would definitely consider lowering dose	Excellent noise texture

The noise standard deviation was estimated in a 128 × 128 ROI within each reconstructed image and used along with the *K*-factor lookup tables to calculate the resulting d'_{gen} for each image. The statistical equivalence between the observer IQ scores for the reference and IR reconstructions was tested with a paired, two-sided *t*-test assuming unequal variance.

6.B. Study 3: results

Figure 8 displays images of the abdominal phantom reconstructed by the reference algorithm and the four levels of iterative reconstruction. The top row displays images from the four levels of iterative reconstruction using the d'_{gen}-AEC method to match the d'_{gen} of the reference protocol. The bottom row displays images from the four iterative reconstruction levels obtained using the existing AEC to match the noise standard deviation of the reference scan. The average observer overall IQ score is displayed for each image along with the $\mathrm{CTDI_{vol}}$.

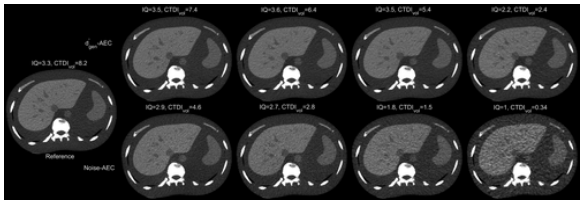

Figure 8 The reference image of the abdominal phantom is displayed at the left side of the figure. The top row displays images generated by the proposed to d'_{gen}-AEC method, where the prescribed noise level was calculated using the *K*-factor lookup tables to match the d'_{gen} of the reference image, and the existing AEC was used to derive the tube current profile to meet that noise level. The bottom row displays images generated by prescribing the same noise level as the reference image. The images, from left to right, represent IR 1, IR 2, IR 3, and IR 4. The mean overall image quality score recorded by the observer and $\mathrm{CTDI_{vol}}$ is displayed above each image. The prescribed and measured noise values for the d'_{gen}-AEC method are given in Table IV.

As seen in Fig. 8, the d'_{gen}-AEC method provided more consistent IQ between the reference algorithm and the four strengths of iterative reconstruction (IR1–IR4) with reduced dose compared to reference scan. For example, the mean IQ score was 3.3 for the reference and 3.5 for the IR3 image produced using d'_{gen}-AEC. Images obtained using the noise-based AEC resulted in lower dose than the d'_{gen}-AEC images but demonstrated reduced IQ compared to the reference scan and the d'_{gen}-AEC images.

Table 4 lists the prescribed noise standard deviation σ_{IR}, noise standard deviation measured in the image σ, the prescribed d'_{gen} values, and the resulting d'_{gen} calculated using the measured noise standard deviation and *K*-factor lookup table. The closer agreement between prescribed and observed d'_{gen} is likely associated with a similar agreement between the measured and prescribed image noise level.

Table 4. The prescribed d'_{gen}, prescribed noise standard deviation, and measured noise standard deviation tabulated for each reconstruction approach in the top row of Fig. 8. The d'_{gen} resulting from the lookup table for the measured noise standard deviation is also presented

	Prescribed σ_{IR}	Measured σ	Prescribed d'_{gen}	Resulting d'_{gen}
Reference	17	17.5	7.5	7.3
IR 1	13.7	15.4	7.5	6.8
IR 2	11.7	13.0	7.5	6.8
IR 3	9.5	10.7	7.5	6.8
IR 4	6.8	8.4	7.5	6.0

Figure 9 plots the observer IQ, noise, and noise texture scores for the reference and iterative reconstruction methods. The proposed d'_{gen}-AEC method resulted in diagnostic IQ, noise, and noise texture scores that were statistically equivalent to the reference scan for IR1-IR3 ($P > 0.37$). The images acquired to match the noise standard deviation of the reference scan demonstrated lower mean IQ score than the reference scan, with the reduction in IQ score statistically significant for IR 3 and IR 4 ($P < 0.005$). For IR4, images produced by d'_{gen}-AEC method had significantly lower IQ scores than the reference scan ($P = 0.003$); however, the images had higher IQ score (IQ = 2.2) than the images resulting from matching the noise standard deviation of the reference scan (IQ = 1). Figure 10 plots the mean observer score of overall IQ against the prescribed and resulting d'_{gen} values.

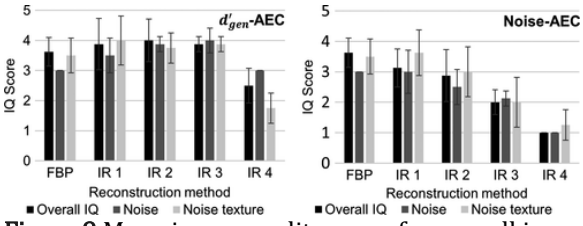

Figure 9 Mean image quality score for overall image quality for diagnosis, noise in the image, and noise texture plotted for range of reconstruction algorithm for images produced by the (left) d'_{gen}-AEC and (right) noise-based AEC methods. The error bars represent the standard deviation of image quality score across the five readers.

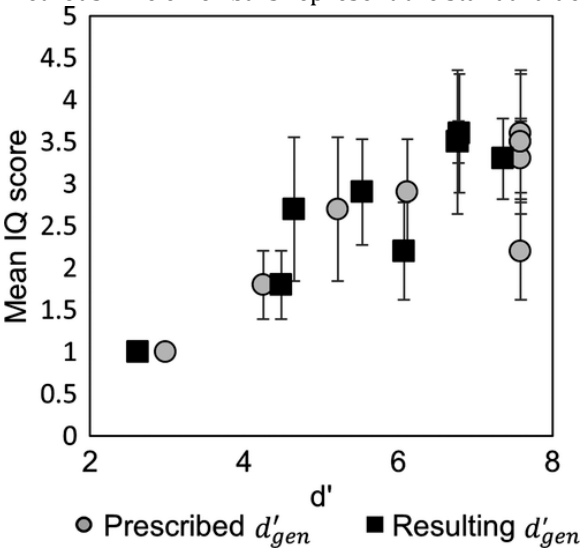

Figure 10 Mean observer score for image quality plotted against the prescribed d'_{gen} and resulting d'_{gen} values. The error bars represent the standard deviation across the five observers.

7 Discussion

This paper proposes a method to determine the noise parameter to input to existing AEC systems to provide consistent IQ across different reconstruction approaches. The results demonstrated that using the d'_{gen}-AEC method provided equivalent IQ to the reference scan for IR 1, IR 2, and IR 3, at reduced dose compared to the reference scan.

For the IR 4 algorithm, the d'_{gen}-AEC method resulted in a d'_{gen} of 4.2 and mean observer IQ score of 2.2, compared to a d'_{gen} of 7.6 and IQ of 3.3 for the reference scan. When an ideal noise-based AEC system was modeled in the study described in Section 4, the lookup table method was able to identify the correct noise level for IR4 to match the d'_{gen} of the reference scan (Fig. 6). When the noise-based AEC was used to derive tube current (Section 5), higher discrepancies between the measured d' and prescribed d'_{gen} were associated with similarly higher discrepancies between prescribed and measured noise standard deviation, particularly evident for IR 4 (Tables 2 and 4). These results suggest that it is difficult for the noise-based AEC to model the relationship between tube current, patient size, and noise level for this iterative algorithm with high level of regularization. Despite this discrepancy, the d'_{gen}-AEC method provided improved IQ compared to the noise-based AEC system for IR 4.

The d'_{gen}-AEC method achieved more consistent IQ at reduced dose compared to the reference scan. The noise-based AEC system provided greater dose reduction than the d'_{gen}-AEC method, however, at reduced IQ compared to the reference scan. If overall lower IQ is acceptable to the radiologist, the reference dose level could also be reduced. These results demonstrate that the dose reduction potential of IR algorithms may be overestimated when matching the image noise standard deviation across algorithms.

In this study, the *K*-factors were calculated as the average value obtained across the studied dose range, since results illustrated in Fig. 2 indicated that the *K*-factors were relatively constant with dose. However, the *K*-factors did indeed decrease at the lower dose range. This reduction in *K*-factor is due to increased blurring that occurs at high noise level, due to increased regularization and potentially electronic noise correction. The error in the assumption of constant *K*-factors at low dose is potentially the cause of the discrepancy between the prescribed d'_{gen} and measured d' at low doses (Fig. 5), which was greater for the ACR phantom with elliptical shell due to reduced detected exposure through larger objects. The MTF and NPS of iterative reconstruction algorithms are known to change with noise level,[26, 34] which would affect the *K*-factors for cases of low-dose acquisition and large object size. This leads to the conclusion that the d'_{gen}-AEC method could potentially be improved in the future by creating separate *K*-factor lookup tables for low-dose ranges that would need to depend on the level of dose reaching the detector and may change with patient size.

This study used a two-dimensional calculation of d' [Eq. 2], due to the method of calculating MTF_{task} from the contrast elements within the ACR phantom.[26] The d'_{gen}-AEC method could be improved in future work by using a three-dimensional d' calculation that takes into account how the IR algorithms differ in spatial resolution along the slice direction. The d'_{gen}-AEC method accounts for the nonlinear response of iterative reconstruction algorithms due to local contrast level, which is a cause of the spatially varying response of iterative reconstruction algorithms. Other factors that cause the MTF or NPS to vary locally are not modeled by the

proposed d'_{gen}-AEC method. MTF and NPS are known to vary locally even for filtered back projection reconstruction, yet these metrics have been widely used to describe overall IQ as a first-order approximation, which is the goal of the proposed method.

A previous study proposed using the CHO to identify the dose setting for an iterative reconstruction algorithm to match the low-contrast detectability of a reference scan.**13** This previous method and our proposed method both aim to provide consistent IQ across different reconstruction approaches. The primary differences are that our proposed d'_{gen}-AEC method can leverage the noise-based AEC system on some scanner models to derive the tube current profile and uses a task-based SNR metric, d', instead of a metric of detection performance (area under the receiver operator characteristic curve: AUC). Because d' represents the signal-to-noise ratio between the observer scores for the signal present and absent conditions, it can be mathematically related to AUC for certain conditions.**37** However, calculating the AUC typically requires more images. Unlike d', AUC saturates at one when the observer score distributions are separated and the signal is reliably detectable by the observer, even as noise level decreases. d' continues to increase as the noise level decreases. Based on the above reasons, we consider it may be more practical to use d' as a general IQ metric for guiding AEC that is less sensitive to accurate modeling of the task object.

The evaluation of the d'_{gen}-AEC method in this study used the 120 HU, 25-mm acrylic Gaussian as the representative task object for driving the derivation of the tube current profile. For the abdominal phantom in Study 3, the results of the d'_{gen}-AEC method could potentially be improved by using a lower contrast task to calculate the K-factors, for example, a 25 HU contrast level as is seen in the liver of the phantom. The size of the task object can be altered by changing the analytical function W_{task}. However, calculating the MTF_{task} for a lower contrast object requires calibration scans at this contrast level. Our goal was to develop a task-based AEC method that is practical to calibrate. The results of this study suggest that the d'_{gen}-AEC method can provide IQ comparable to the reference scan without requiring exact knowledge of the imaging task. However, Fig. 3 demonstrates that accurate modeling of task shape may be more important for small, high-contrast objects. Future studies are needed to investigate the performance of the d'_{gen}-AEC method for other applications, such as cardiac imaging or lung imaging, where small objects with high contrast may drive the tube current profile. It may be possible for a clinical application to be driven by multiple task requirements. In this case, it may be beneficial to calculate the required tube current for each task independently and then pick the higher tube current to ensure adequate IQ for all tasks.

The proposed d'_{gen}-AEC method can be implemented by the user on any scanner with a noise-based AEC method. For each reconstruction algorithm, a K-factor lookup table should be calculated using the methods described in Section 3, which involve scanning a uniform phantom for estimating NPS and a phantom with elements at desired contrast levels for estimating MTF_{task}. The results in Fig. 2 suggest that performing calibration at one dose setting may be acceptable, although improvements could be obtained with additional low-dose lookup tables. K-factors for tasks of different size and shape could be obtained by changing the analytical task function, W_{task}. For each protocol, a reference standard deviation must be determined that produces acceptable IQ for the reference algorithm. This reference noise standard deviation could be based on existing protocol tables, as this reference noise level is currently input to the scanner as the noise index, or the noise level could be estimated in a reference image of acceptable IQ.

Using the lookup table for the reference algorithm and the measured noise standard deviation in a reference image of acceptable IQ, the user would calculate the reference d'_{gen} value. The lookup table for the desired iterative algorithm would then be used to calculate the noise standard deviation that should be prescribed for the iterative algorithm to meet this IQ level. The reference reconstruction need not be based on filtered back projection. The *K*-factor lookup tables along with Eq. 7 could be used to convert the desired noise standard deviations between any two algorithms.

While the proposed method was designed specifically for scanners with noise-based AEC systems, a d'_{gen}-based method could potentially be developed for scanners with other AEC systems. For scanners that take a reference tube-current-time-product value as input to the AEC, a lookup table of weighting factors could potentially be calibrated to convert reference mAs values between different reconstruction algorithms, with the goal of maintaining constant detectability.

This study presents a preliminary feasibility study of the proposed d'_{gen}-AEC method. Quantitative results and conclusions are limited to the algorithms and phantoms that were evaluated. Future work is needed to further investigate the performance of the d'_{gen}-AEC method for additional object sizes and contrast levels, as well as additional reconstruction algorithms. The proposed method could be applied in future work to provide consistent IQ across other changes in scan parameters, for example, tube voltage setting.

8 Conclusions

This study investigated a novel AEC method, based on a generalized detectability index, to provide more consistent IQ across image reconstruction approaches. The proposed method can be implemented on CT scanners with noise-based AEC by using a lookup table of scaling factors to calculate the noise standard deviation needed for an iterative algorithm to meet a reference detectability index. The results of the phantom study provide preliminary evidence that the proposed d'_{gen}-AEC can produce consistent IQ across different iterative reconstruction approaches, with reduced dose compared to the reference scan.

Conflicts of Interest

Parag Khobragade and Taly Gilat Schmidt receive research funding from GE Healthcare. Jiahua Fan, Franco Rupcich, and Dominic Crotty are employees of GE Healthcare.

References

1Nguyen PK, Wu JC. Radiation exposure from imaging tests: is there an increased cancer risk? *Expert Rev Cardiovasc Ther*. 2011; **9**: 177– 183.

2 National Council on Radiation Protection and Measurements. *Ionizing Radiation Exposure of the Population of the United States*. Bethesda, MD: National Council on Radiation Protection and Measurements; 2009.

3Söderberg M, Gunnarsson M. Automatic exposure control in computed tomography – an evaluation of systems from different manufacturers. *Acta Radiol*. 2010; **51**: 625– 634.

4Gandhi D, Crotty DJ, Stevens GM, Schmidt TG. Technical note: phantom study to evaluate the dose and image quality effects of a computed tomography organ-based tube current modulation technique. *Med Phys*. 2015; **42**: 6572– 6578.

5Silva AC, Lawder HJ, Hara A, Kujak J, Pavlicek W. Innovations in CT dose reduction strategy: application of the adaptive statistical iterative reconstruction algorithm. *Am J Roentgenol*. 2010; **194**: 191– 199.

6Prakash P, Kalra MK, Digumarthy SR, et al. Radiation dose reduction with chest computed tomography using adaptive statistical iterative reconstruction technique. *J Comput Assist Tomogr*. 2010; **34**: 40– 45.
7Singh S, Kalra MK, Gilman MD, et al. Adaptive statistical iterative reconstruction technique for radiation dose reduction in chest CT: a pilot study. *Radiology*. 2011; **259**: 565– 573.
8Bittencourt MS, Schmidt B, Seltmann M, et al. Iterative reconstruction in image space (IRIS) in cardiac computed tomography: initial experience. *Int J Cardiovasc Imaging*. 2011; **27**: 1081– 1087.
9Szucs-Farkas Z, Bensler S, Torrente JC, Cullmann JL, Vock P, Schindera ST. Nonlinear three-dimensional noise filter with low-dose ct angiography: effect on the detection of small high-contrast objects in a phantom model. *Radiology*. 2011; **258**: 261– 269.
10Bai M, Chen J, Raupach R, Suess C, Tao Y, Peng M. Effect of nonlinear three-dimensional optimized reconstruction algorithm filter on image quality and radiation dose: validation on phantoms. *Med Phys*. 2008; **36**: 95– 97.
11Yu L, Fletcher JG, Shiung M, et al. Radiation dose reduction in pediatric body CT using iterative reconstruction and a novel image-based denoising method. *AJR Am J Roentgenol*. 2015a; **205**: 1026– 1037.
12Brisse HJ, Madec L, Gaboriaud G, et al. Automatic exposure control in multichannel CT with tube current modulation to achieve a constant level of image noise: experimental assessment on pediatric phantoms. *Med Phys*. 2007; **34**: 3018– 3033.
13Favazza CP, Yu L, Leng S, Kofler JM, McCollough CH. Automatic exposure control systems designed to maintain constant image noise. *J Comput Assist Tomogr*. 2015; **39**: 1.
14Iball GR, Moore AC, Crawford EJ. A routine quality assurance test for CT automatic exposure control systems. *J Appl Clin Med Phys*. 2016; **17**: 291– 306.
15Martin CJ, Sookpeng S. Setting up computed tomography automatic tube current modulation systems. *J Radiol Prot*. 2016; **36**: R74– R95.
16Qi LP, Li Y, Tang L, et al. Evaluation of dose reduction and image quality in chest CT using adaptive statistical iterative reconstruction with the same group of patients. *Br J Radiol*. 2012; **85**: 906– 911.
17Chen B, Christianson O, Wilson JM, Samei E. Assessment of volumetric noise and resolution performance for linear and nonlinear CT reconstruction methods. *Med Phys*. 2014; **41**: 071909.
18Li K, Tang J, Chen G-H. Statistical model based iterative reconstruction (MBIR) in clinical CT systems: experimental assessment of noise performance. *Med Phys*. 2014; **41**: 041906.
19Boedeker KL, McNitt-Gray MF. Application of the noise power spectrum in modern diagnostic MDCT: part II. Noise power spectra and signal to noise. *Phys Med Biol*. 2007; **52**: 4047– 4061.
20Solomon J, Wilson J, Samei E. Characteristic image quality of a third generation dual-source MDCT scanner: noise, resolution, and detectability. *Med Phys*. 2015a; **42**: 4941– 4953.
21Khobragade P, Fan J, Rupcich F, Crotty DJ, Schmidt TG. Application of fractal dimension for quantifying noise texture in computed tomography images. *Med Phys*. 2018a; **45**: 3563– 3573.
22Schindera ST, Odedra D, Raza SA, et al. Iterative reconstruction algorithm for CT: can radiation dose be decreased while low-contrast detectability is preserved? *Radiology*. 2013; **269**: 511– 518.
23Kim M, Lee JM, Yoon JH, et al. Adaptive iterative dose reduction algorithm in CT: effect on image quality compared with filtered back projection in body phantoms of different sizes. *Korean J Radiol*. 2014; **15**: 195– 204.
24Tseng H-W, Fan J, Kupinski MA, Sainath P, Hsieh J. Assessing image quality and dose reduction of a new x-ray computed tomography iterative reconstruction algorithm using model observers. *Med Phys*. 2014; **41**: 071910.
25Vaishnav JY, Jung WC, Popescu LM, Zeng R, Myers KJ. Objective assessment of image quality and dose reduction in CT iterative reconstruction. *Med Phys*. 2014; **41**: 071904.
26Richard S, Husarik DB, Yadava G, Murphy SN, Samei E. Towards task-based assessment of CT performance: system and object MTF across different reconstruction algorithms. *Med Phys*. 2012a; **39**: 4115– 4122.
27Yu L, Vrieze TJ, Leng S, Fletcher JG, McCollough CH. Technical Note: measuring contrast- and noise-dependent spatial resolution of an iterative reconstruction method in CT using ensemble averaging. *Med Phys*. 2015b; **42**: 2261– 2267.

28McCollough CH, Yu L, Kofler JM, et al. Degradation of CT low-contrast spatial resolution due to the use of iterative reconstruction and reduced dose levels. *Radiology*. 2015; **276**: 499– 506.
29Favazza CP, Ferrero A, Yu L, Leng S, McMillan KL, McCollough CH. Use of a channelized Hotelling observer to assess CT image quality and optimize dose reduction for iteratively reconstructed images. *J Med Imaging*. 2017; **4**: 31213.
30Burgess AE. Statistically defined backgrounds: performance of a modified nonprewhitening observer model. *J Opt Soc Am A*. 1994; **11**: 1237.
31Sharp P, Metz C, Wagner R, Myers K, Burgess A. Medical Imaging-The Assessment of Image Quality ICRU Report 54. Bethesda, MD: ICRU; 1996.
32Christianson O, Chen JJS, Yang Z, et al. An improved index of image quality for task-based performance of CT iterative reconstruction across three commercial implementations. *Radiology*. 2015; **275**: 725– 734.
33Solomon J, Mileto A, Ramirez-Giraldo JC, Samei E. Diagnostic performance of an advanced modeled iterative reconstruction algorithm for low-contrast detectability with a third-generation dual-source multidetector CT scanner: potential for radiation dose reduction in a multireader study. *Radiology*. 2015b; **275**: 735– 745.
34Samei E, Richard S. Assessment of the dose reduction potential of a model-based iterative reconstruction algorithm using a task-based performance metrology. *Med Phys*. 2014; **42**: 314– 323.
35Gang GJ, Stayman JW, Ehtiati T, Siewerdsen JH. Task-driven image acquisition and reconstruction in cone-beam CT. *Phys Med Biol*. 2015 Mar 24; **60**: 3129.
36Khobragade P, Fan J, Rupcich F, Crotty DJ, Schmidt TG. Automated exposure control for CT using a task-based image quality metric. In: Medical Imaging 2018: Physics of Medical Imaging. International Society for Optics and Photonics; 2018b. page 1057316.
37Barrett HH, Myers KJ, Hoeschen C, Kupinski MA, Little MP. Task-based measures of image quality and their relation to radiation dose and patient risk. *Phys Med Biol*. 2015; **60**: R1– R75.